Electromagnetic Information Theory Motivated Near-Field Channel Model

Zhongzhichao Wan, Jieao Zhu, and Linglong Dai, *Fellow, IEEE*
Department of Electronic Engineering, Tsinghua University
Beijing National Research Center for Information Science and Technology (BNRist), Beijing 100084, China
E-mails: {wzzc20, zja21}@mails.tsinghua.edu.cn; daill@tsinghua.edu.cn

2024 IEEE International Symposium on Information Theory (ISIT) | 979-8-3503-8284-6/24/$31.00 ©2024 IEEE | DOI: 10.1109/ISIT57864.2024.10619301

***Abstract*—Electromagnetic information theory (EIT) is one of the important topics for 6G communication due to its potential to reveal the performance limit of wireless communication systems. For EIT, the research foundation is reasonable and accurate channel modeling. Existing channel modeling works for EIT in non-line-of-sight (NLoS) scenario focus on far-field modeling, which can not accurately capture the characteristics of the channel in near-field. In this paper, we propose the near-field channel model for EIT based on electromagnetic scattering theory. We model the channel by using non-stationary Gaussian random fields and derive the analytical expression of the correlation function of the fields. Furthermore, we analyze the characteristics of the proposed channel model, including how the parameters of the scattering field affect the degrees of freedom (DoF).**

***Index Terms*—Electromagnetic information theory (EIT), near field, channel modeling, Gaussian random field, channel estimation.**

I. Introduction

To improve the system performance, various promising technologies, including reconfigurable intelligent surfaces (RISs) [1], [2], continuous-aperture multiple-input multiple-output (CAP-MIMO) [3], [4], and near-field communications [5], [6], have been proposed for sixth-generation (6G) communication. All these technologies are trying to explore new sources of DoF or capacity gain. These performance gains actually come from more accurate understanding and precise manipulation of electromagnetic fields which convey information [7]. Therefore, combining classical electromagnetic theory and information theory to provide modeling and capacity analysis tools is of great importance for exploring the fundamental performance limit of wireless communication systems, which leads to the interdisciplinary subject called electromagnetic information theory (EIT) [8]. By integrating deterministic physical theory and stochastic mathematically theory [9], EIT is expected to provide new insights into system models, degrees of freedom, capacity limits, etc., from the electromagnetic perspective.

A. Prior works

The existing research directions of EIT includes channel modeling [10]–[12], DoF analysis [13]–[15], mutual information and capacity analysis [16]–[18], etc. Among these directions, channel modeling is the fundamental part. Without precise channel model, DoF and capacity of EIT can not be accurately analyzed.

For the channel modeling schemes of EIT, one approach is line-of-sight (LoS) modeling scheme derived directly from Maxwell's equations, and the channel is expressed by the Green's function in free space [10], [11] or considering reflection from a surface [12]. Another approach considers NLoS channel, which obeys the electromagnetic scattering theory [19]. Compared to LoS channel, NLoS channel is more general. Due to the complexity and uncertainty of the scattering environment, the NLoS channel is often modeled by random fields, whose statistical characteristics are derived from the scattering environment [20]. For example, an isotropic statistical channel model is derived in [21], which can be viewed as an extension of the traditional independent and identically distributed (i.i.d.) Rayleigh fading channel model. Furthermore, a more general scheme for constructing small-scale fading channel is provided in [22], where the received electromagnetic field is expanded by Fourier plane waves. This model corresponds to far-field scattering scenario and provides a useful way of expanding the channel in the wavenumber domain. An extended work [23] further derives approximate analytical correlation function based on [22], leading to a non-isotropic channel model.

The above works use spatially stationary assumption to build channel models for EIT, which suits far-field scenarios better than near-field scenarios. However, for the use of middle-band, millimeter-wave and terahertz technologies, or extremely large aperture [24], such approximation is not accurate, which may introduce non-negligible errors in DoF and capacity analysis, as well as system design such as channel estimation. Therefore, an accurate channel modeling scheme for EIT in near-field scenarios is needed.

B. Our contributions

Different from the existing works, in this paper, we propose a near-field channel modeling scheme for EIT based on random field, and derive the analytical expression of the correlation function of the channel. Specifically, the contributions of this paper are summarized as follows:

- We propose a near-field channel model for EIT based on the electromagnetic scattering theory. The channel is modeled by Gaussian random fields to capture the statistical characteristics of the scattering field.
- We derive the approximate analytical expression of the correlation function of the channel. Moreover, we verify

its approximation accuracy by numerical simulation.

- We analyze the characteristics of the proposed near-field model. We show how to generate one sample of the random field channel model. Then, we show how the parameters of the model affects the degree of freedom (DoF) of the channel. Finally, we show the sparsity of the model in the wavenumber domain.

Notation: bold uppercase characters denote matrices; bold lowercase characters denote vectors; the dot $\cdot$ denotes the scalar product of two vectors, or the matrix-vector multiplication. $\mathbb{E}[x]$ denotes the mean of random variable x; ϵ_0 is the permittivity of a vacuum, μ_0 is the permeability of a vacuum, and c is the speed of light in a vacuum; $*$ denotes the convolution operation; $J_m(x)$ is the m_{th} order Bessel function of the first kind. $\lfloor x \rfloor$ represents rounding x down.

II. Electromagnetic Model for Scattering Field

Maxwell's equations are the fundamental physical laws of the electromagnetic system. For the characteristics of the scattering system, we can consider the scatterers as spatial non-uniformity of the electromagnetic characteristics like permittivity ϵ and permeability μ in the space. From the Maxwell's equations and the time-harmonic assumption [25] we have

$$\nabla \times \mathbf{E}(\mathbf{r}) = \mathrm{j}\omega\mu(\mathbf{r})\mathbf{H}(\mathbf{r}), \tag{1a}$$

$$\nabla \times \mathbf{H}(\mathbf{r}) = -\mathrm{j}\omega\epsilon(\mathbf{r})\mathbf{E}(\mathbf{r}) + \mathbf{J}(\mathbf{r}), \tag{1b}$$

$$\nabla \cdot (\epsilon(\mathbf{r})\mathbf{E}(\mathbf{r})) = \rho(\mathbf{r}), \tag{1c}$$

$$\nabla \cdot (\mu(\mathbf{r})\mathbf{H}(\mathbf{r})) = 0, \tag{1d}$$

where $\epsilon(\mathbf{r})$, $\mu(\mathbf{r})$ and $\rho(\mathbf{r})$ represents the permittivity, permeability and charge density at the position $\mathbf{r}$.

By ignoring the polarization of electromagnetic fields and adopting the scalar wave form as in [26], we can obtain the following equation from [19]

$$(\nabla^2 + k^2(\mathbf{r}))E(\mathbf{r}) = q(\mathbf{r}), \tag{2}$$

where $k(\mathbf{r}) = \omega\sqrt{\mu(\mathbf{r})\epsilon(\mathbf{r})}$ represents the inhomogeneous media over a finite domain V according to [19], and $q(\mathbf{r}) = \mathrm{j}\omega\mu(\mathbf{r})J(\mathbf{r})$ represents the source field. Outside the domain V, the wavenumber $k(\mathbf{r})$ equals $k_0 = \omega\sqrt{\mu_0\epsilon_0}$. By using the Green's function $g(\mathbf{r},\mathbf{r}') = \frac{e^{\mathrm{j}k\|\mathbf{r}-\mathbf{r}'\|}}{4\pi\|\mathbf{r}-\mathbf{r}'\|}$ which is the solution of $(\nabla^2 + k^2)g(\mathbf{r},\mathbf{r}') = -\delta(\mathbf{r}-\mathbf{r}')$, we can derive

$$E(\mathbf{r}) = -\int_{V_s} g(\mathbf{r},\mathbf{r}')q(\mathbf{r}')\mathrm{d}\mathbf{r}' + \int_V g(\mathbf{r},\mathbf{r}')(k^2(\mathbf{r}') - k_0^2) E(\mathbf{r}')\mathrm{d}\mathbf{r}', \tag{3}$$

where V_s is the source region which generates the signal, and $E(\mathbf{r}')$ is the induced electric field in the inhomogeneous regions in the space. The equation (3) is an extension from the 2-dimensional case in [27]. Here we can view the first item in (3) as the line-of-sight component of the field which is fixed and well-studied. Then we will focus on the second item in (3) which highly relies on the characteristics of the inhomogeneity of the space. The inhomogeneity of the space depends on the complicated factors such as surface structure and material properties of the medium which are hard to analytically model and may change over time. Therefore, a statistical model will be more suitable to capture the characteristics of the field than deterministic modeling scheme.

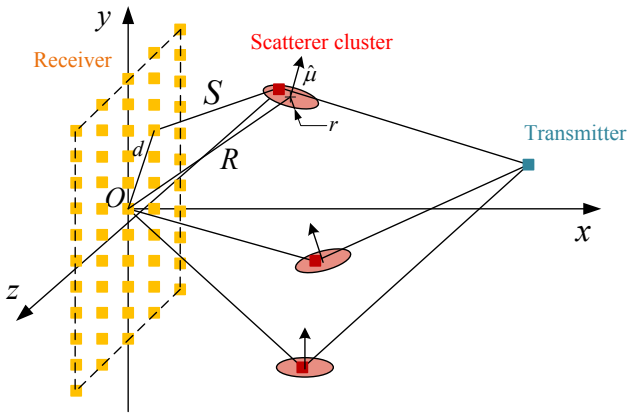

Fig. 1. The three-dimensional near-field statistical channel modeling where the scatterers are located in solid circles.

III. Channel Model Based on Non-Stationary Random Fields

In this section we will derive the channel model for EIT based on the electromagnetic scattering theory explained in the above section. The channel is modeled as Gaussian random fields to tolerate the uncertainty of the inhomogeneity of the space [28]. Since in our model the received field can be viewed as weighted superposition of spherical waves other than plane waves in [22], it is suitable for both near-field and far-field communications by considering distances between antenna array and scatterers besides the azimuth and elevation angles.

A. Mathematical derivation of the analytical model

By omitting the first item in (3) which represents the deterministic line-of-sight component, we have

$$R_E(\mathbf{r}_1,\mathbf{r}_2) = \mathbb{E}\Big[\int_V \int_V g(\mathbf{r}_1,\mathbf{r}_1')g^*(\mathbf{r}_2,\mathbf{r}_2')(k^2(\mathbf{r}_1') - k_0^2)(k^2(\mathbf{r}_2') - k_0^2)E(\mathbf{r}_1')E^*(\mathbf{r}_2')\mathrm{d}\mathbf{r}_1'\mathrm{d}\mathbf{r}_2'\Big]. \tag{4}$$

To derive a closed-form expression of the channel model we need to have some assumptions on the scattering field to do simplifications on (4). Considering the uncertainty of the inhomogeneity of the space, simplified models need to be used for the field correlation on the scatter surfaces for the ease of analysis. In the literature, some models have already been proposed. For example, delta function type of field spatial correlation is discussed in [29], [30] and [31], which implies an ideal but mathematically friendly assumption that the material properties are varying instantaneously in the spatial domain. More complex model like exponential type of field spatial correlation is discussed in [32]. Angular delta function as the spectrum of the field is proposed in

[33]. For simplicity, we adopt delta function as the spatial correlation of the fields on the scattering surface, leading to $\mathbb{E}\left[E(\mathbf{r}_1')E^*(\mathbf{r}_2')\right] = \beta\delta(\mathbf{r}_1'-\mathbf{r}_2')$. Then, the channel correlation function reduces to

$$R_E(\mathbf{r}_1,\mathbf{r}_2) = \beta\int_V g(\mathbf{r}_1,\mathbf{r}')g^*(\mathbf{r}_2,\mathbf{r}')(k^2(\mathbf{r}')-k_0^2)^2\mathrm{d}\mathbf{r}'. \tag{5}$$

We further assume that the scattering region V is distributed in a solid circle, centering at $\mathbf{d}$ and perpendicular to $\hat{\boldsymbol{\mu}}$, which means that $\hat{\boldsymbol{\mu}}^{\mathrm{T}}(\mathbf{r}'-\mathbf{d}) = 0$. The practical meaning of such assumption is that the scatterer faces receivers at a certain angle. The radius of the circle is r_s. For the item $(k^2(\mathbf{r}')-k_0^2)^2$, we view it as the gain of electromagnetic waves reflected from the surface of scatterer determined by the electromagnetic characteristics of the scattering surface. Specifically, we model it by

$$f(\mathbf{r}') = (k^2(\mathbf{r}')-k_0^2)^2 = \frac{a+1}{\pi r_s^{2a+2}}(r_s^2-\rho^2)^a, \tag{6}$$

where $\boldsymbol{\rho} = \mathbf{r}'-\mathbf{d}$, $\rho = \|\boldsymbol{\rho}\|$, and a is a parameter characterizing the concentration of scatterer around the central point. When $a = 0$, the scattering region is a uniform circular surface. When $a \to -1$, the scatterer approximates a ring. When $a \to +\infty$, the scattering region shrinks to a single point. Then, we can express the correlation function by

$$R_E(\mathbf{r}_1,\mathbf{r}_2) = \beta\int_V \frac{e^{\mathrm{j}k\|\mathbf{r}_1-\mathbf{r}'\|}}{4\pi\|\mathbf{r}_1-\mathbf{r}'\|}\frac{e^{-\mathrm{j}k\|\mathbf{r}_2-\mathbf{r}'\|}}{4\pi\|\mathbf{r}_2-\mathbf{r}'\|}f(\mathbf{r}')\mathrm{d}\mathbf{r}'. \tag{7}$$

To facilitate the derivation procedure, we choose a coordinate rotation $\mathbf{T}$ which satisfies $\mathbf{T}\hat{\boldsymbol{\mu}} = \hat{\mathbf{e}}_x$. Then we have a new rotated coordinate where $\boldsymbol{\mu}$ is the x axis. The center of the scatterer is located at $\mathbf{Td}$, and the receiving locations are $\mathbf{Tr}_1$ and $\mathbf{Tr}_2$. One point in the scattering region is located at $\mathbf{Td}+\mathbf{T}\boldsymbol{\rho}$, where $\mathbf{T}\boldsymbol{\rho} = [\rho\cos\theta, \rho\sin\theta, 0]$. Here we denote two directions $\hat{\boldsymbol{\mu}}_1$ and $\hat{\boldsymbol{\mu}}_2$ perpendicular to $\hat{\boldsymbol{\mu}}$, which satisfies $\hat{\boldsymbol{\mu}}_1^{\mathrm{T}}\hat{\boldsymbol{\mu}}_2 = 0$. Then we can denote $\mathbf{Td}$ by $[\mathbf{d}\cdot\hat{\boldsymbol{\mu}}, \mathbf{d}\cdot\hat{\boldsymbol{\mu}}_1, \mathbf{d}\cdot\hat{\boldsymbol{\mu}}_2]$. Similarly, we have $\mathbf{Tr} = [\mathbf{r}\cdot\hat{\boldsymbol{\mu}}, \mathbf{r}\cdot\hat{\boldsymbol{\mu}}_1, \mathbf{r}\cdot\hat{\boldsymbol{\mu}}_2]$. The point in the scattering point is located at $[\mathbf{d}\cdot\hat{\boldsymbol{\mu}}, \mathbf{d}\cdot\hat{\boldsymbol{\mu}}_1+\rho\cos\theta, \mathbf{d}\cdot\hat{\boldsymbol{\mu}}_2+\rho\sin\theta]$. The rotated coordinate system is shown in Fig. 2. The distance between $\mathbf{r}$ and $\mathbf{r}'$ is (8) where

$$\begin{aligned} A(\mathbf{r}) =& 1+\left(\frac{r}{d}\right)^2 - 2\frac{r}{d}\Bigg((\hat{\mathbf{d}}\cdot\hat{\boldsymbol{\mu}})(\hat{\mathbf{r}}\cdot\hat{\boldsymbol{\mu}}) \\ &+ (\hat{\mathbf{d}}\cdot\hat{\boldsymbol{\mu}}_1)(\hat{\mathbf{r}}\cdot\hat{\boldsymbol{\mu}}_1) + (\hat{\mathbf{d}}\cdot\hat{\boldsymbol{\mu}}_2)(\hat{\mathbf{r}}\cdot\hat{\boldsymbol{\mu}}_2)\Bigg), \end{aligned} \tag{9}$$

and

$$\begin{aligned} B(\mathbf{r},\hat{\boldsymbol{\rho}}) =& \hat{\mathbf{d}}\cdot\hat{\boldsymbol{\mu}}_1\cos\theta + \hat{\mathbf{d}}\cdot\hat{\boldsymbol{\mu}}_2\sin\theta - \frac{r}{d}\hat{\mathbf{r}}\cdot\hat{\boldsymbol{\mu}}_1\cos\theta \\ &- \frac{r}{d}\hat{\mathbf{r}}\cdot\hat{\boldsymbol{\mu}}_2\sin\theta. \end{aligned} \tag{10}$$

Through mathematical derivations and simplifications, we can derive the spatial correlation function of the channel in the following lemma:

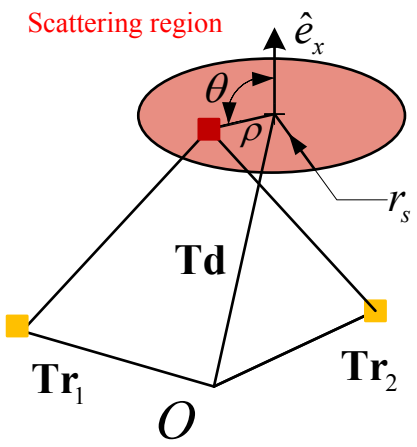

Fig. 2. The rotated coordinate system with $\mathbf{T}\hat{\boldsymbol{\mu}} = \hat{\mathbf{e}}_x$.

Lemma 1 (Correlation function of the channel): Assuming that $r_s \ll d$, the correlation function of the channel can be approximated by

$$\begin{aligned} \tilde{R}(\mathbf{r}_1,\mathbf{r}_2) =& \frac{\beta}{8\pi^2 d^2\sqrt{A(\mathbf{r}_1)A(\mathbf{r}_2)}}e^{\mathrm{j}\frac{2\pi}{\lambda}R\left(\sqrt{A(\mathbf{r}_1)}-\sqrt{A(\mathbf{r}_2)}\right)} \\ &(a+1)2^a\Gamma(a+1)(\sqrt{C}r_s)^{-(a+1)}J_{a+1}(\sqrt{C}r_s), \end{aligned} \tag{11}$$

where

$$\begin{aligned} C =& \left(\frac{2\pi}{\lambda}\right)^2\left(\frac{\hat{\mathbf{d}}\cdot\hat{\boldsymbol{\mu}}_1}{\sqrt{A(\mathbf{r}_1)}} - \frac{\hat{\mathbf{d}}\cdot\hat{\boldsymbol{\mu}}_1}{\sqrt{A(\mathbf{r}_2)}} - \frac{r_1}{d}\frac{\hat{\mathbf{r}}_1\cdot\hat{\boldsymbol{\mu}}_1}{\sqrt{A(\mathbf{r}_1)}} \right. \\ &\left. + \frac{r_2}{R}\frac{\hat{\mathbf{r}}_2\cdot\hat{\boldsymbol{\mu}}_1}{\sqrt{A(\mathbf{r}_2)}}\right)^2 \\ &+ \left(\frac{2\pi}{\lambda}\right)^2\left(\frac{\hat{\mathbf{d}}\cdot\hat{\boldsymbol{\mu}}_2}{\sqrt{A(\mathbf{r}_1)}} - \frac{\hat{\mathbf{d}}\cdot\hat{\boldsymbol{\mu}}_2}{\sqrt{A(\mathbf{r}_2)}} - \frac{r_1}{d}\frac{\hat{\mathbf{r}}_1\cdot\hat{\boldsymbol{\mu}}_2}{\sqrt{A(\mathbf{r}_1)}} \right. \\ &\left. + \frac{r_2}{d}\frac{\hat{\mathbf{r}}_2\cdot\hat{\boldsymbol{\mu}}_2}{\sqrt{A(\mathbf{r}_2)}}\right)^2. \end{aligned} \tag{12}$$

For the channel with multiple scatterers, the correlation function can be expressed by

$$R(\mathbf{r}_1,\mathbf{r}_2) = \sum_{k=1}^{M}\tilde{R}_k(\mathbf{r}_1,\mathbf{r}_2), \tag{13}$$

where each $\tilde{R}_k(\mathbf{d}_1,\mathbf{d}_2)$ is constructed according to **Lemma 1**.

B. Numerical verification of the accuracy of the analytical model

In this subsection, we will show the accuracy of the analytical correlation function in **Lemma 1**. We set the direction of the scattering region to the center of the array as $\hat{\mathbf{d}} = [\frac{1}{\sqrt{3}}, \frac{1}{\sqrt{3}}, \frac{1}{\sqrt{3}}]$. The scattering region is perpendicular to the direction $\hat{\boldsymbol{\mu}} = [-\frac{1}{\sqrt{3}}, \frac{1}{\sqrt{3}}, -\frac{1}{\sqrt{3}}]$. The concentration

$$\begin{aligned}\|\mathbf{r}-\mathbf{r}'\| &= \sqrt{(\mathbf{d}\cdot\hat{\boldsymbol{\mu}}-\mathbf{r}\cdot\hat{\boldsymbol{\mu}})^2+(\mathbf{d}\cdot\hat{\boldsymbol{\mu}}_1+\rho\cos\theta-\mathbf{r}\cdot\hat{\boldsymbol{\mu}}_1)^2+(\mathbf{d}\cdot\hat{\boldsymbol{\mu}}_2+\rho\sin\theta-\mathbf{r}\cdot\hat{\boldsymbol{\mu}}_2)^2} \\ &= d\sqrt{A(\mathbf{r})+2\frac{\rho}{d}B(\mathbf{r},\hat{\boldsymbol{\rho}})+\left(\frac{\rho}{d}\right)^2},\end{aligned} \tag{8}$$

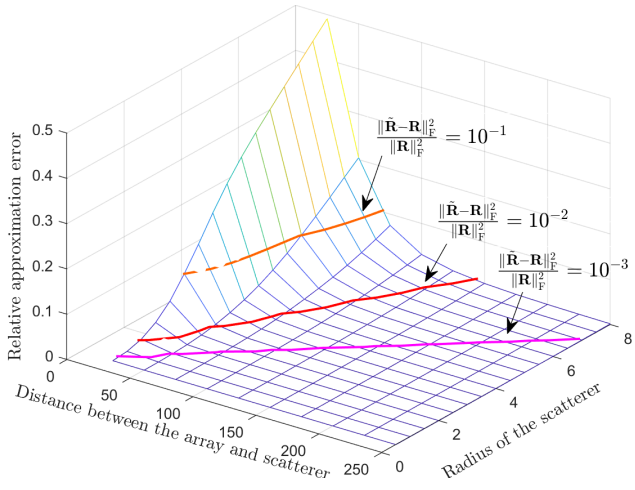

Fig. 3. The correlation function plotted from the approximated analytical expression.

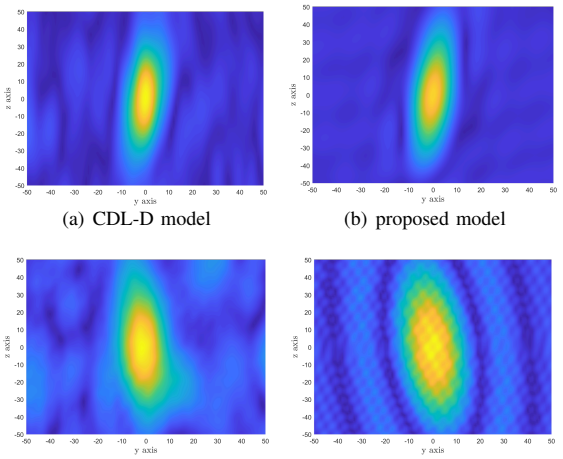

(a) CDL-D model (b) proposed model

(c) CDL-A model (d) proposed model

Fig. 4. Comparison between the field correlation of CDL-A, CDL-D and the proposed model.

parameter on the scatterer cluster is set to $a = 0$, which corresponds to uniform distribution on the circle. For the correlation between the received fields at two positions on the receiving array, we fix one position at the center of the array and another position at $[0, \pm n_y d_y, \pm n_z d_z]\,\mathrm{m}$, where $n_y, n_z \in \mathcal{I}_N$, $\mathcal{I}_N = \{1, \cdots, 100\}$, $d_y = d_z = 0.025\,\mathrm{m}$. The wavelength λ is set to $0.05\,\mathrm{m}$. We plot $\frac{\|\tilde{\mathbf{R}}-\mathbf{R}\|_F^2}{\|\mathbf{R}\|_F^2}$, which is the relative error between the approximated correlation matrix and the accurate correlation matrix, in Fig. 3. We can find that the approximation error is negligible compared to the value of the corresponding correlation function when d is large enough or r_s is small enough. For example, when d is larger than $100\,\mathrm{m}$ and r_s is smaller than $3.5\,\mathrm{m}$, the relative approximation error is below 1%, which is tolerable in most cases.

C. Fitness to the statistics of classical CDL model

In this part we will show the fitness of the proposed model to the statistics of standard 3GPP TR 38.901 CDL model [34]. Since CDL model is now widely used in 5G new radio (5G NR) scenarios, the rationality of the proposed analytical correlation function of the channel model can be verified if it can well fit the statistics of the CDL model. We simulate the field correlation of CDL-A and CDL-D model, which represent strong scattering and weak scattering scenarios separately. For the antenna array, we adopt 101×101 array with $\lambda/8$ antenna spacing. We use the proposed analytical model with two scatterers to fit the field correlation of the CDL model, which is shown in Fig. 4. It is shown that the proposed model can fit the statistical characteristics of CDL models with few parameters, especially for CDL-D model, which verifies its correctness and generalization capability. The benefits of the proposed model is that it is analytical and can be used to obtain the field correlation between any two positions by direct and quick calculation.

IV. Characteristics of the Proposed Channel Model

In this section, we will analyze and show the characteristics of the derived channel model, which can reveal how the scattering environment affects the system performance and the sparsity of the channel in the wavenumber domain.

A. One realization of the random field

For the derived correlation function $R(\mathbf{r}, \mathbf{r}')$, we have the following expansion $R = \sum_{i=1}^{\infty} \lambda_i \phi(\mathbf{r}) \phi^*(\mathbf{r}')$ from Mercer's theorem, where $\phi(\mathbf{r})$ is the solution of the following integral equation

$$\lambda_i \phi(\mathbf{r}) = \int_V R(\mathbf{r}, \mathbf{r}') \phi(\mathbf{r}) \mathrm{d}\mathbf{r}, \tag{14}$$

according to [35]. Then the received field can be constructed by its Karhunen-Loève expansion $E(\mathbf{r}) = \sum_{i=1}^{\infty} \xi_i \phi(\mathbf{r})$, where $\lambda_i = \mathbb{E}[\xi_i \xi_i^*]$. For a noisy received field $Y(\mathbf{r}) = E(\mathbf{r}) + N(\mathbf{r})$ where $R_N(\mathbf{r}, \mathbf{r}') = \sigma^2 \delta(\mathbf{r} - \mathbf{r}')$, the information that can be obtained from the received field is $I(E; Y) = \sum_i \log(1 + \frac{\lambda_i}{\sigma^2})$ [18].

If we consider discrete samples of the continuous fields, for a $N_y \times N_z$ array at the receiver, we can construct a correlation

matrix $\mathbf{R} \in \mathbb{C}^{(N_y N_z)\times(N_y N_z)}$, where $\mathbf{R}_{i,j} = R(\mathbf{r}_i, \mathbf{r}_j)$, $\mathbf{r}_i = \left[0, \lfloor \frac{i-1}{N_z} \rfloor - \frac{N_y-1}{2}, \mathrm{mod}\,(i-1, N_z) - \frac{N_z-1}{2}\right]$, and $\mathbf{r}_j = \left[0, \lfloor \frac{j-1}{N_z} \rfloor - \frac{N_y-1}{2}, \mathrm{mod}\,(j-1, N_z) - \frac{N_z-1}{2}\right]$. From the correlation function of the received field, we can generate the channel by $\mathbf{h} = \mathbf{R}^{\frac{1}{2}}\mathbf{N}$, where $\mathbf{R}^{\frac{1}{2}}$ is the Cholesky decomposition of the correlation matrix $\mathbf{R}$, and $\mathbf{N} \sim \mathcal{CN}(0, \mathbf{I})$.

B. Impact of the parameters on the analytical model

In this part, we will discuss the impact of parameters on the accuracy and performance of the analytical model. First we will show how scatterer size r_s reflect the accuracy of the model and when it can not be neglected. It is well known that the Rayleigh distance, also called as Fraunhofer distance, is $d = \frac{8r_{\mathrm{m}}^2}{\lambda}$, where d is the distance from the antenna array, and $r_{\mathrm{m}} = \max\|\mathbf{r}\|$ is the radius of the antenna array [36]. The Rayleigh distance is defined by the distance where $\frac{\pi}{8}$ phase error is observed on the antenna array. If we further consider the size of the scatterer, we have the channel response as $h(\mathbf{r}', \mathbf{r}) = e^{\mathrm{j}\frac{2\pi}{\lambda}\|\mathbf{r}'-\mathbf{r}\|}$, where $\mathbf{r}' = \mathbf{d} + \boldsymbol{\rho}$ is the position of one point on the scatterer. In **Lemma 2** we extend the Rayleigh distance considering scatterers

Lemma 2 (Extension of Rayleigh distance considering scatterer size): The size of scatterer can be neglected when $r_{\mathrm{s}} \leqslant \frac{\lambda}{16}$ and $d \leqslant \frac{8(r_{\mathrm{s}}+r_{\mathrm{m}})^2}{\lambda - 16 r_s}$. Otherwise, the scatterer size should be considered in the channel model. Under this scenario, when $d \leqslant \frac{8(r_{\mathrm{s}}+r_{\mathrm{m}})^2}{\lambda}$, the scatterer and the antenna array are in the near-field region. When $d \geqslant \frac{8(r_{\mathrm{s}}+r_{\mathrm{m}})^2}{\lambda}$, the scatterer and the antenna array are in the far-field region.

From **Lemma 2** we know that unless the scatterer is small enough (for frequency of 1 GHz the radius of the scatterer should be smaller than 0.0187 m), neglecting the size of the scatterer and simply view it as a point will be inaccurate. Therefore, considering parameters of scatterer is of necessity for channel modeling especially in near-field communication scenarios.

Then, we will discuss how the parameters influence the performance of the system from the degree of freedom (DoF) perspective. The DoF of the channel depends on the eigenvalue distribution of the model. If the eigenvalue decay rate is slow, there exist multiple subchannels that can support communication at a certain rate, leading to higher DoF. On the contrary, if few eigenvalues are obviously larger than other eigenvalues, the DoF will be low [21]. Then, we plot the eigenvalues of the correlation matrix when the radius and shape of the scattering region vary in Fig. 5 and Fig. 6. We can observe that the DoF of the channel will increase with the radius r of the scatterer, and decrease when a increases.

V. Conclusion

In this paper, we propose the near-field channel model for EIT based on electromagnetic scattering theory. Then, we derive the analytical expression of the correlation function of the fields and verifies the accuracy of the analytical result by numerical simulation. Finally, we analyze the characteristics of the derived channel model, which reveal the influence of the channel parameters on the channel DoF.

Further work can be done by integrating the proposed model and traditional near-field model where some scatterers are invisible to part of the array.

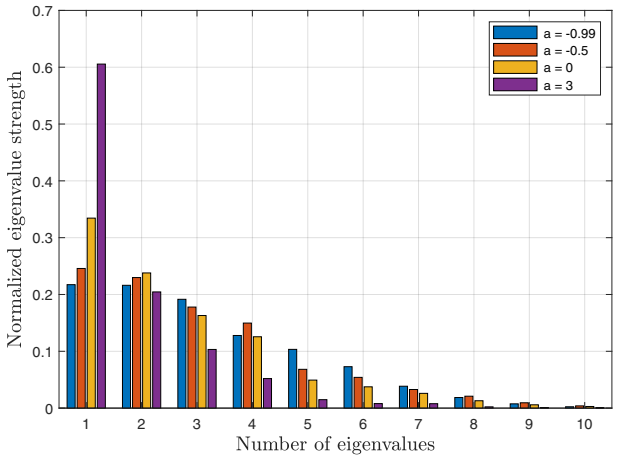

Fig. 5. The eigenvalues of the correlation matrix in decreasing order with $\mathbf{d}$ fixed to $[-100, 100, -100]$ m, $\boldsymbol{\mu}$ fixed to $[-\frac{1}{\sqrt{3}}, \frac{1}{\sqrt{3}}, -\frac{1}{\sqrt{3}}]$, and $r = 5$ m. The concentration parameter a varies.

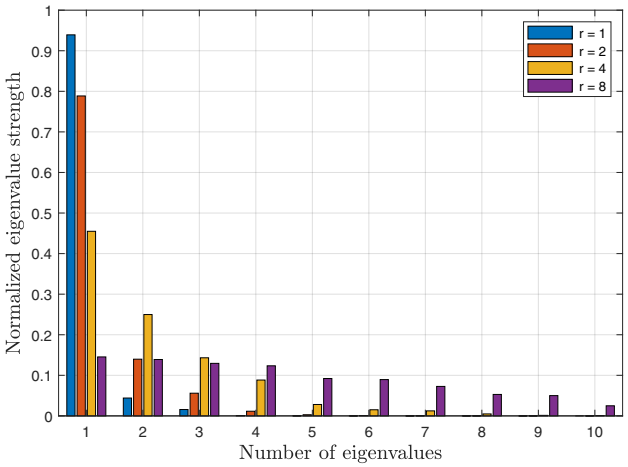

Fig. 6. The eigenvalues of the correlation matrix in decreasing order with $\mathbf{d}$ fixed to $[-100, 100, -100]$ m, $\boldsymbol{\mu}$ fixed to $[-\frac{1}{\sqrt{3}}, \frac{1}{\sqrt{3}}, -\frac{1}{\sqrt{3}}]$, and $a = 0$. The radius r varies.

Acknowledgment

This work was supported in part by the National Key Research and Development Program of China (Grant No. 2020YFB1807201), in part by the National Natural Science Foundation of China (Grant No. 62031019).

REFERENCES

[1] E. Basar, M. Di Renzo, J. De Rosny, M. Debbah, M.-S. Alouini, and R. Zhang, "Wireless communications through reconfigurable intelligent surfaces," *IEEE Access*, vol. 7, pp. 116 753–116 773, Aug. 2019.

[2] Z. Wang, Z. Liu, Y. Shen, A. Conti, and M. Z. Win, "Location awareness in beyond 5G networks via reconfigurable intelligent surfaces," *IEEE J. Sel. Areas Commun.*, vol. 40, no. 7, pp. 2011 – 2025, Mar. 2022.

[3] C. Huang, S. Hu, G. C. Alexandropoulos, A. Zappone, C. Yuen, R. Zhang, M. Di Renzo, and M. Debbah, "Holographic MIMO surfaces for 6G wireless networks: Opportunities, challenges, and trends," *IEEE Wireless Commun.*, vol. 27, no. 5, pp. 118–125, Jul. 2020.

[4] Z. Zhang and L. Dai, "Pattern-division multiplexing for multi-user continuous-aperture MIMO," *IEEE J. Sel. Areas Commun.*, vol. 41, no. 8, pp. 2350–2366, Jun. 2023.

[5] M. Cui, Z. Wu, Y. Lu, X. Wei, and L. Dai, "Near-field MIMO communications for 6G: Fundamentals, challenges, potentials, and future directions," *IEEE Comm. Mag.*, vol. 61, no. 1, pp. 40–46, Sep. 2022.

[6] Z. Wu and L. Dai, "Multiple access for near-field communications: SDMA or LDMA?" *IEEE J. Sel. Areas Commun.*, vol. 41, no. 6, pp. 1918–1935, May 2023.

[7] M. Chafii, L. Bariah, S. Muhaidat, and M. Debbah, "Twelve scientific challenges for 6G: Rethinking the foundations of communications theory," *IEEE Comm. Surveys Tut.*, Feb. 2023.

[8] M. D. Migliore, "Horse (electromagnetics) is more important than horseman (information) for wireless transmission," *IEEE Trans. Antennas Propag.*, vol. 67, no. 4, pp. 2046–2055, Apr. 2018.

[9] J. Zhu, Z. Wan, L. Dai, M. Debbah, and H. V. Poor, "Electromagnetic information theory: Fundamentals, modeling, applications, and open problems," *IEEE Wireless Commun.*, early access, Jan. 2024, doi: 10.1109/MWC.019.2200602.

[10] T. Gong, L. Wei, C. Huang, Z. Yang, J. He, M. Debbah, and C. Yuen, "Holographic MIMO communications with arbitrary surface placements: Near-field LoS channel model and capacity limit," *arXiv preprint arXiv:2304.05259*, 2023.

[11] L. Wei, C. Huang, G. C. Alexandropoulos, Z. Yang, J. Yang, E. Wei, Z. Zhang, M. Debbah, and C. Yuen, "Tri-polarized holographic MIMO surfaces for near-field communications: Channel modeling and precoding design," *IEEE Trans. Wireless Commun.*, early access, 2023.

[12] A. Pizzo, A. Lozano, S. Rangan, and T. L. Marzetta, "Wide-aperture MIMO via reflection off a smooth surface," *IEEE Trans. Wireless Commun.*, vol. 22, no. 8, pp. 5229–5239, Jan. 2023.

[13] O. Bucci and G. Franceschetti, "On the spatial bandwidth of scattered fields," *IEEE Trans. Antennas Propag.*, vol. 35, no. 12, pp. 1445–1455, Dec. 1987.

[14] O. M. Bucci and G. Franceschetti, "On the degrees of freedom of scattered fields," *IEEE Trans. Antennas Propag.*, vol. 37, no. 7, pp. 918–926, Jul. 1989.

[15] M. Franceschetti, "On Landau's eigenvalue theorem and information cut-sets," *IEEE Trans. Inf. Theory*, vol. 61, no. 9, pp. 5042–5051, Jul. 2015.

[16] M. A. Jensen and J. W. Wallace, "Capacity of the continuous-space electromagnetic channel," *IEEE Trans. Antennas Propag.*, vol. 56, no. 2, pp. 524–531, Feb. 2008.

[17] W. Jeon and S.-Y. Chung, "Capacity of continuous-space electromagnetic channels with lossy transceivers," *IEEE Trans. Inf. Theory*, vol. 64, no. 3, pp. 1977–1991, Dec. 2017.

[18] Z. Wan, J. Zhu, Z. Zhang, L. Dai, and C.-B. Chae, "Mutual information for electromagnetic information theory based on random fields," *IEEE Trans. Commun.*, vol. 71, no. 4, pp. 1982 – 1996, Feb. 2023.

[19] W. C. Chew, *Waves and fields in inhomogenous media*. John Wiley & Sons, 1999, vol. 16.

[20] A. Pizzo, L. Sanguinetti, and T. L. Marzetta, "Fourier plane-wave series expansion for holographic MIMO communications," *IEEE Trans. Wireless Commun.*, vol. 21, no. 9, pp. 6890–6905, Mar. 2022.

[21] E. Björnson and L. Sanguinetti, "Rayleigh fading modeling and channel hardening for reconfigurable intelligent surfaces," *IEEE Wireless Commun. Lett.*, vol. 10, no. 4, pp. 830–834, Dec. 2020.

[22] A. Pizzo, T. L. Marzetta, and L. Sanguinetti, "Spatially-stationary model for holographic MIMO small-scale fading," *IEEE J. Sel. Areas Commun.*, vol. 38, no. 9, pp. 1964–1979, Sep. 2020.

[23] Ö. T. Demir, E. Björnson, and L. Sanguinetti, "Channel modeling and channel estimation for holographic massive MIMO with planar arrays," *IEEE Wireless Commun. Lett.*, vol. 11, no. 5, pp. 997–1001, May 2022.

[24] Y. Liu, Z. Wang, J. Xu, C. Ouyang, X. Mu, and R. Schober, "Near-field communications: A tutorial review," *IEEE Open Journal of the Communications Society*, pp. 1999–2049, Aug. 2023.

[25] F. K. Gruber and E. A. Marengo, "New aspects of electromagnetic information theory for wireless and antenna systems," *IEEE Trans. Antennas Propag.*, vol. 56, no. 11, pp. 3470–3484, Nov. 2008.

[26] A. Pizzo, L. Sanguinetti, and T. L. Marzetta, "Spatial characterization of electromagnetic random channels," *IEEE Open Journal of the Communications Society*, vol. 3, pp. 847–866, Apr. 2022.

[27] L. Li, L. G. Wang, F. L. Teixeira, C. Liu, A. Nehorai, and T. J. Cui, "DeepNIS: Deep neural network for nonlinear electromagnetic inverse scattering," *IEEE Trans. Antennas Propag.*, vol. 67, no. 3, pp. 1819–1825, Mar. 2018.

[28] G. Franceschetti and D. Riccio, *Scattering, natural surfaces, and fractals*. Elsevier, 2006.

[29] H. Cabayan and R. Murphy, "Scattering of electromagnetic waves by rough perfectly conducting circular cylinders," *IEEE Trans. Antennas Propag.*, vol. 21, no. 6, pp. 893–895, Nov. 1973.

[30] R. Osgood Iii, S. Sinha, J. Freeland, Y. Idzerda, and S. Bader, "X-ray scattering from magnetically and structurally rough surfaces," *Journal of magnetism and magnetic materials*, vol. 198, pp. 698–702, Jun. 1999.

[31] J. C. Dainty, "The statistics of speckle patterns," in *Progress in optics*. Elsevier, 1977, vol. 14, pp. 1–46.

[32] K. Tang, R. A. Dimenna, and R. O. Buckius, "Regions of validity of the geometric optics approximation for angular scattering from very rough surfaces," *International Journal of Heat and Mass Transfer*, vol. 40, no. 1, pp. 49–59, Oct. 1996.

[33] F. Ticconi, L. Pulvirenti, N. Pierdicca, and V. Zhurbenko, "Models for scattering from rough surfaces," *Electromagnetic waves*, vol. 10, pp. 203–226, 2011.

[34] 3GPP TR, "Study on channel model for frequencies from 0.5 to 100 ghz," *3GPP TR 38.901 version 14.0.0 Release*, Dec. 2019.

[35] J. Mercer, "Functions of positive and negative type, and their connection with the theory of integral equations," *Philos. Trans. Roy. Soc. London*, vol. 209, no. 441-458, pp. 415–446, Jan. 1909.

[36] K. T. Selvan and R. Janaswamy, "Fraunhofer and Fresnel distances: Unified derivation for aperture antennas." *IEEE Antennas and Propag. Mag.*, vol. 59, no. 4, pp. 12–15, Aug. 2017.